Supporting Information

Visualizing morphogenesis through instability formation in 4-D printing

Dong Wu[†, ‡], Jiaqi Song[†, ‡], Zirui Zhai[§], Mutian Hua[†], Cheolgyu Kim[†], Imri Frenkel[†], Hanqing Jiang[§], Ximin He[†,*]

[†] Department of Materials Science and Engineering, University of California, Los Angeles (UCLA), Los Angeles, California 90095, United States

[§] School for Engineering of Matter, Transport and Energy, Arizona State University, Tempe, Arizona 85281, United States

[‡] D.W. and J.S. contributed equally.

*Corresponding author.

E-mail address: ximinhe@ucla.edu (X. H)

S1. Theory and simulation

The shape transition of hydrogels is a transient multi-physics process, which involves mass diffusion of water into/out of the gel and large deformation of the gel network. To model this complicated behavior, the inhomogeneous field theory that couples large deformation and mass diffusion developed by Hong *et al.*[1] and the finite element method developed by Wang *et al.*[2] were used and implemented in the environment of commercial multi-physics modeling software COMSOL.

In the inhomogeneous field theory of gel, a standard approach in continuum mechanics is used for the kinematics of the network. The stress-free initial state is taken as the reference state. In large deformation, deformation gradient

$$\mathbf{F} = \frac{\partial \mathbf{x}(\mathbf{X}, t)}{\partial \mathbf{X}}$$

is used to map between the reference state (with coordinate **X**) and the current state (with coordinate **x**(**X**, *t*)).

For mass diffusion, the conservation of mass can be expressed as

$$\frac{\partial C}{\partial t} + \frac{\partial J_K}{\partial X_K} = 0,$$

where C is the nominal solvent concentration, and **J** is the nominal flux. An equivalent way to express the flux is through the true flux j_i

$$j_i n_i da = J_K N_K dA,$$

where da and dA are the areas of the element, while n_i and N_K are the unit vectors normal to the interface, in the current state and the reference state, respectively. Using the conservation of mass in an integration form,

$$\frac{d}{dt}\int_V C dV + \int_A J_K N_K dA = 0,$$

and divergence theorem, the differential form in true flux can be expressed as

$$\frac{1}{\det \mathbf{F}} \frac{\partial C}{\partial t} + \frac{\partial j_i}{\partial x_i} = 0.$$

The nominal concentration C relates to the deformation via the condition of incompressibility

$$1 + \nu C = \det \mathbf{F},$$

where ν is the volume per small molecule, and true concentration of solvent relates to the nominal concentration via

$$c \det \mathbf{F} = C .$$

The true flux is given by the gradient of the chemical potential,

$$j_i = -cD(T)\frac{\partial \mu}{\partial x_i}$$

where *D(T)* is the temperature dependent intrinsic diffusivity and μ is the normalized chemical potential (by $k_B T$) of the solvent inside the gel. Thus, the conservation of mass can be derived as

$$\frac{1}{\det \mathbf{F}}\frac{\partial(\det \mathbf{F}-1)}{\partial t} + \frac{\partial\left[-\dfrac{(\det \mathbf{F}-1)D(T)}{\det \mathbf{F}}\dfrac{\partial \mu}{\partial x_i}\right]}{\partial x_i} = 0$$

This equation can be directly implemented using the heat transfer equation or coefficient form of the PDE interface of COMSOL.

A user-defined hyperelastic material node under solid mechanics interface can be used to describe the constitutive relation. One choice of the free energy density is the Flory-Huggins model, where the normalized nominal free energy density $\hat{W}(\mathbf{F})$ is given by[1]

$$\hat{W}(\mathbf{F}) = \frac{W(\mathbf{F},C)}{\dfrac{k_B T}{\nu}} = \frac{1}{2}N\nu\left[F_{iK}F_{iK} - 3 - 2\log(\det \mathbf{F})\right] - \left[(\det \mathbf{F}-1)\log\left(\frac{\det \mathbf{F}}{\det \mathbf{F}-1}\right) + \frac{\chi}{\det \mathbf{F}-1}\right] - \mu(\det \mathbf{F}-1)$$

where $N\nu$ is a dimensionless materials property representing the shear modulus of the dry polymer and ν is molecule volume of water. The shear modulus of the dry polymer $Nk_B T$ is related to the normalized shear modulus by $Nk_B T = \frac{k_B T}{\nu} N\nu$. *T* is the temperature, k_B is the Boltzmann constant and χ is the temperature dependent dimensionless materials properties representing the enthalpy of mixing. All the materials parameters can be determined or derived from the experiment results (Table S1). With the solid mechanics and the PDE interface of COMSOL, the transient analysis of the gels with coupled mass diffusion and large deformation can now be formed. More details of this implementation can be found.[1-3]

2D instability simulation of pumpkin models

To simplify the modeling of pumpkin models and focus on the instability phenomenon, a 2D plane stress condition is assumed here. It is also assumed that a surface energy is associated with the free boundary of the gel,[4] which creates a surface traction $\vec{t}$ in the current configuration a

$$\vec{t} = t_0 \cdot \vec{n}$$

where $\vec{n}$ is the outer unit vector associated with the free boundary, and t_0 is set as 0.02 N/m for all the 2D instability simulations. The surface traction is applied after the gel system is fully swelled. The outer boundary is set as no displacement restriction and zero chemical potential. The displacement and chemical potential fields have continued values between the two layers of gels. Hundreds of quadratic elements have been used for both displacement and chemical potential field discretization.

3D growing simulations of various plant models

The hydrogels are modeled with real dimensions of the initial gel states. Thousands of linear elements have been used for both displacement and chemical potential field discretization. All the outer boundaries are without displacement restriction and at zero chemical potential. The displacement and chemical potential fields have continued value between different gels. Because of geometric symmetry, 1/8 of the model is used for the simulation of the flower.

Table S1. Parameters used in the simulation

Parameter	Description	Value
ρ_{drygel}	Density of dry gel	1.395g·cm^{-3}
ρ_{water}	Density of water	1000 kg·m^{-3}
T	Water temperature	293.15 K
k_B	Boltzmann constant	$1.38064852 \times 10^{-23} J \cdot K^{-1}$
v_{water}	Molecular volume of water	2.99×10^{-29} m^3

ν_{drygel}	Poisson's ratio of dry gel	0.5
λ_0	Length swelling ratio of all gels from dry state to initial state	1.5
$E_{3.5s}$	Young's modulus of 3.5 s gel at initial state	23.8 kPa
E_{4s}	Young's modulus of 4 s gel at initial state	38.6 kPa
E_{8s}	Young's modulus of 8 s gel at initial state	186 kPa
E_{10s}	Young's modulus of 10 s gel at initial state	295 kPa
λ_{3s}	Length swelling ratio of 3 s gel from initial state to final state	1.77
$\lambda_{3.5s}$	Length swelling ratio of 3.5 s gel from initial state to final state	1.73
λ_{4s}	Length swelling ratio of 4 s gel from initial state to final state	1.70
λ_{8s}	Length swelling ratio of 8 s gel from initial state to final state	1.40
λ_{10s}	Length swelling ratio of 10 s gel from initial state to final state	1.37

S2. Design of the pumpkin model

A Computer-aided design (CAD) model was utilized to print the pumpkin models with various core-shell radius ratios. The profile of the CAD model is shown as Figure S1. Different core-shell ratios were achieved by only tuning the radius of the core, A. The other parameters, including the height of the model and the diameter of the outer radius of the shell, were fixed to eliminate the potential interference.

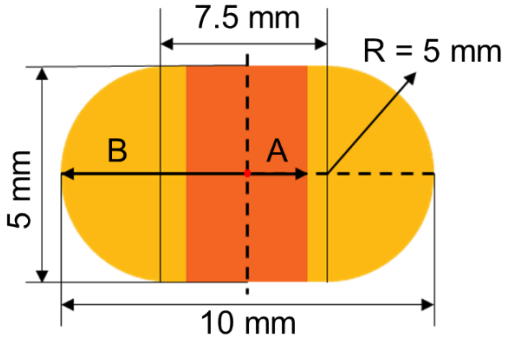

Figure S1. Profile of the CAD model. The core-shell radius ratio is tuned by the radius of the core, A, which is the only varying parameter in this profile. The core-shell ratio of the model (A/B) varies from 0.2 to 0.6 in this work.

S3. Analytical Calculation

To understand the roles of different parameters in the buckling formation of the pumpkin model, including the swelling ratio difference and the core/shell ratio, a well-known model involving three states has been adopted as shown in Figure S2.[5]

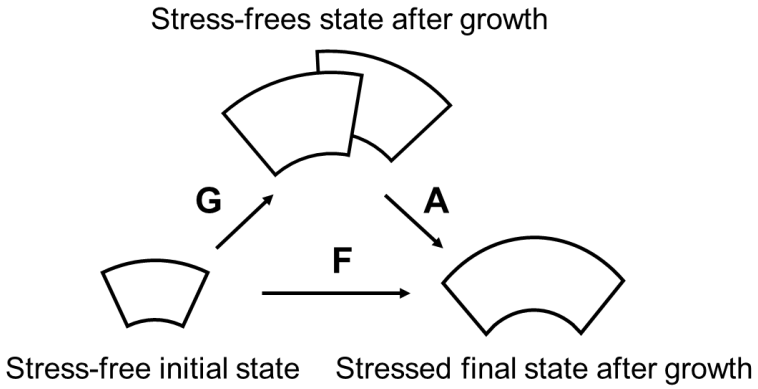

Figure S2. A model of the swelling of hydrogel includes three states: the stress-free initial state before growth, the stress-free state after growth, and the stressed final state after growth. Three tensors are utilized to map one state to another: the growth tensor **G**, the deformation tensor **A**, and the deformation gradient **F**, which are related to each other by **F**=**AG**. Reproduced with permission from reference 6.[6] Copyright 2011 IOP Publishing Ltd.

The initial state of hydrogel is considered as stress-free while the final state, which can be achieved after growth, is taken as stressed. Besides, a stress-free state after unconstrained and homogeneous growth is assumed to analyze the growth process.

The stress-free growth is characterized by the growth tensor, $\mathbf{G} = \mathrm{diag}[g_r, g_\theta, g_z]$, and the deformation attributed to the constrain imposed by the surrounding elements is characterized by the deformation tensor, $\mathbf{A} = \mathrm{diag}[\alpha_r, \alpha_\theta, \alpha_z]$. The deformation gradient of the final state to the initial state, $\mathbf{F} = \mathrm{diag}[\lambda_r, \lambda_\theta, \lambda_z]$, can be achieved by the multiplication of the growth tensor and the deformation tensor: $\mathbf{F} = \mathbf{AG}$, where r is the radial direction, θ is the circumferential direction and z is the longitudinal direction.

Assuming that the deformation is elastic and incompressible, $\det(A) = 1$, then

$$\det(F) = \det(G) = \lambda_r \lambda_\theta \lambda_z = g_r g_\theta g_z$$

Therefore, the principal stretches in deformation gradient can be written as

$$\lambda_r = \frac{g_r g_\theta g_z}{\lambda_\theta \lambda_z} = g_r \alpha_r$$

$$\lambda_\theta = \frac{l_r}{l_R} = \frac{r \cdot \theta}{R \cdot \theta} = \frac{r}{R} = g_\theta \alpha_\theta$$

$$\lambda_z = g_z \alpha_z \quad (\lambda_z = 1 \text{ if there is no deformation in z direction})$$

where R and r are the distance between the same arbitrary element in shell and the center of the concentric circles before and after swelling, l_r and l_R are the corresponding arc length.

Previously, Jin *et al.* has reported the analysis of the crease formation in the soft tissue growing outside the non-swelling rigid core.[6] Based on their model, we went further to analyze the buckling formation of the core-shell structure, in which both the core and the shell swell while shell can swell more than the core. Due to the swelling of both the core and the shell, the 2-step swelling process is proposed as shown in Figure S3.

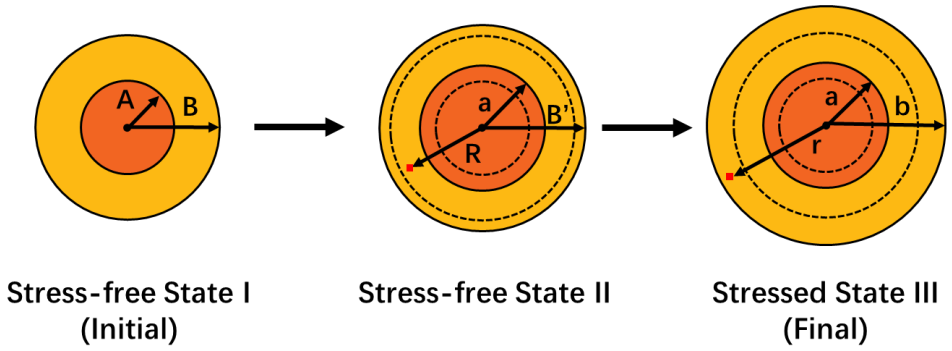

Figure S3. The swelling process is divided into 2 steps involving 3 different states: the initial stress-free State I; the stress-free State II after the homogeneous growth of the core and the shell with the same growth ratio, g_{core}; the final stressed state after complete growth of the model.

The initial state, denoted as **State I**, is taken as stress-free. Both the core and the shell are assumed to swell with the same ratio, g_{core}, simultaneously and homogeneously to a stress-free **State II**:

$$\mathrm{a} = g_{core} A \qquad (1)$$

$$B' = g_{core} B \qquad (2)$$

Define g as the relative growth ratio from stress-free **State II** to stressed **State III**:

$$g_r = g_\theta = g_z = \frac{g_{shell}}{g_{core}} = g$$

The principal stretches will be:

$$\lambda_r = \frac{g_r g_\theta g_z}{\lambda_\theta} = \frac{g^3}{\lambda_\theta};\ \lambda_\theta = \frac{l_r}{l_R} = \frac{r \cdot \theta}{R \cdot \theta} = \frac{r}{R};\ \lambda_z = 1$$

The field of deformation r(R) is determined by:

$$r^2 - a^2 = g_r g_\theta g_z (R^2 - a^2)$$

At the surface $\mathrm{r} = \mathrm{b}$ and $R = B'$, then

$$b^2 - a^2 = g_r g_\theta g_z \left(B'^2 - a^2\right)$$

$$b^2 = g_r g_\theta g_z \left(B'^2 - a^2\right) + a^2 = g^3 \left(B'^2 - a^2\right) + a^2$$

The critical condition for the onset of circumferential creases at the surface of the shell is $\alpha_r/\alpha_\theta = 2.4$, or

$$\frac{\alpha_r}{\alpha_\theta} = \left(\frac{\lambda_r}{g_r}\right)/\left(\frac{\lambda_\theta}{g_\theta}\right) = \left(\frac{g_\theta g_z}{\lambda_\theta}\right)/\left(\frac{\lambda_\theta}{g_\theta}\right) = {g_\theta}^2 g_z B'^2/b^2 = g^3 B'^2/\left(g^3\left(B'^2 - a^2\right) + a^2\right) \qquad (3)$$

Put (1) and (2) into (3), then

$$\frac{\alpha_r}{\alpha_\theta} = g^3 B^2/(g^3(B^2 - A^2) + A^2) = 2.4 \qquad (4)$$

which can also be written as

$$g^3 \Big/ \left(\left(\frac{A}{B}\right)^2 - g^3 \left(\left(\frac{A}{B}\right)^2 - 1 \right) \right) = 2.4$$

As a result, the function $g\left(\frac{A}{B}\right)$ can be achieved as

$$g = \sqrt[3]{\frac{2.4}{2.4 - 1.4\left(\frac{A}{B}\right)^{-2}}}$$

which is plotted as Figure 5(f).

To further investigate the influence of the deformation in z direction on the critical condition of surface buckling, here we introduce λ_z into the calculation. Therefore, the equation (4) can be rewritten as

$$\frac{\alpha_r}{\alpha_\theta} = g^3 B^2/(\lambda_z(g^3(B^2 - A^2) + A^2)) = 2.4$$

The critical relative growth ratio, g, is plotted versus A/B with different λ_z shown as

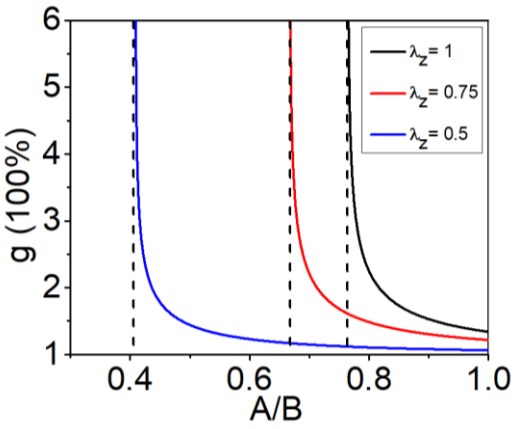

Figure S4. The critical relative growth ratio, g, for onset of the surface buckling as a function of A/B for isotropic growth with different deformation in z direction. (black: $\lambda_z = 1$; red: $\lambda_z = 0.75$; blue: $\lambda_z = 0.5$).

S4. Printing pumpkin model with a hollow core

Pumpkins are commonly regarded as hollow structures, which are different from our solid-core model. To further validate the mechanism of buckling formation in our model, a hollow-core model was printed. The core-shell ratio of this model is 6/10. The shell was cured for 4s and the core was cured for 10s. The hollow core was created by printing ring patterns with a radius ratio of 5/6 (instead of circles) for the 11^{st} ~ 40^{th} layers out of the totally 50 layers and printing (solid) circle patterns for the top and bottom layers to form the two closed ends, *i.e.* the stem and the base of the pumpkin model. Thus, an empty space was created at the center of the core. As Figure S5 shows, buckling occurred on such a hollow-core structure in a similar fashion as occurred with the solid-core structures shown in Figure 1-4. Despite the wall of the tubular core was thin, the core was still strong enough to provide the swelling mismatch and the polar constrain to the whole pumpkin model, which are considered as the essential factors for the buckling formation. Hence, this indicates our solid-core structures are good representative of the real pumpkin in terms of buckling behaviors. In another word, the similarity of buckling behaviors of the hollow- and solid-core structures proves that the key conditions for buckling occurrence are the mismatch between the core and the shell in swelling ratio and modulus, as well as the constraint boundary at the two polar ends of the 3D model.

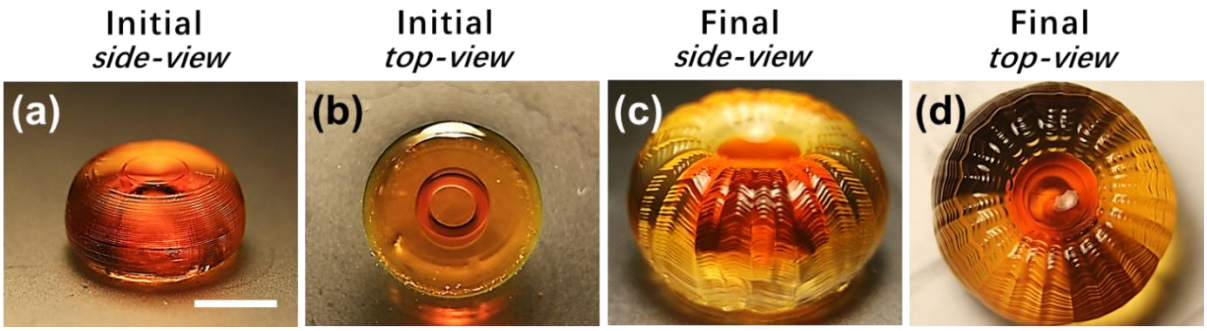

Figure S5. The images of the printed pumpkin model with a hollow core, specifically a 4s-cured shell and a 10s-cured closed-tube core: (a) side-view, (b) top-view of the initial state; (c) side-view and (d) top-view of the final state. Similar buckling formed with such a hollow-core structure as well, proving that the key factors for buckling are swelling mismatch and polar constrain, regardless of the filling of the core. The core-shell ratio of the model is 6/10. The radius ratio of the tubular core is 5/6. The hollow part ranges from the 11st to the 40th layer while the other layers are solid. The scale bar is 5 mm.

S5. Printing patterns of different biomimetic structures

2D flat layered structures were printed, rinsed with ethanol and then immersed in buffer solution to mimic the morphologic formation of four different plants. The thickness of each layer is 0.1 mm. As shown in Figure S6, an 8-layer thin disk with a 3s-cured shell (a) and a 10s-cured core (e) was printed to lead to wave-like shape mimicking cabbage leaves. A structure with a rigid core (f) and double-layer petals (b) was printed to mimic chrysanthemum. Each layer for the core were cured for 10s while for the petals were printed for 8s for the first 2 layers and 3s for the other 4 layers. Rigid lines and curves within soft matrixes were printed to mimic leaves of rose (c), (g) and Bauhinia pods (d), (h). The lines were cured for 15 second each layer while the matrixes were cured for 4s.

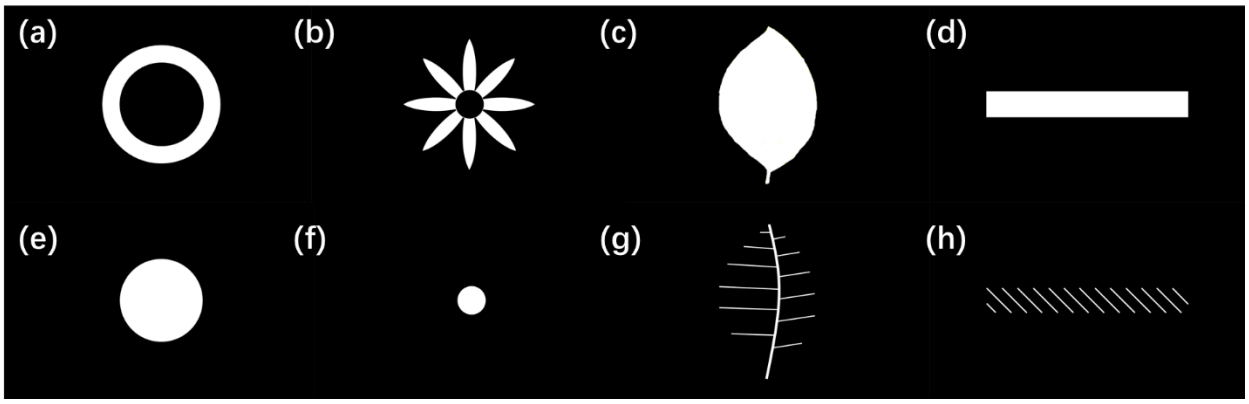

Figure S6. Projected patterns of four different biomimetic structures: (a) a shell and (e) a core mimicking cabbage flowers/leaves; (b) petals and (f) a core of chrysanthemum; (c) mesophyll and (g) veins of leaves of rose; (d) a strip and (h) ridges mimicking helix strips of Bauhinia pods.

S6. Reversibility of the synthetic morphogenesis process

To test the reversibility of the process, different methods have been tried to bring the buckling model back to its original state, including immersing it in ethanol and different pH conditions as well as drying in air.

The reverse process can be achieved by drying the pumpkin model in air or immersing it in ethanol. As Figure S7 shows the pumpkin models shrink back to their initial as-printed size and the buckle disappeared. The morphologies are slightly different from the original ones, because the original state contains only ethanol in the hydrogel network, whereas the shrunken models from drying in air and ethanol contains phosphate salts precipitated from the buffer solution, and the latter also contains ethanol inside the gel.

By changing the surrounding buffer from pH 7 to pH 3-4.5, the hydrogel shrunk, and the buckling disappeared as well, although cracking occurred with the gel network arising from the delamination between the shell and the core. Such breakdown of the structure can be attributed to the internal stress induced by the mismatch between core and shell in shrinkage as well as the non-uniform shrinkage inside either core or shell. It is expected, by improving the mechanical property of the hydrogel, a full reversibility can be also achieved with a tougher gel.

Subsequently, by soaking the shrunken pumpkin model from drying and ethanol back in water, the complete cycle of swelling and buckling ↔ de-swelling and de-buckling ↔ re-swelling and re-buckling was be achieved, which demonstrated the reversibility of the deformation process.

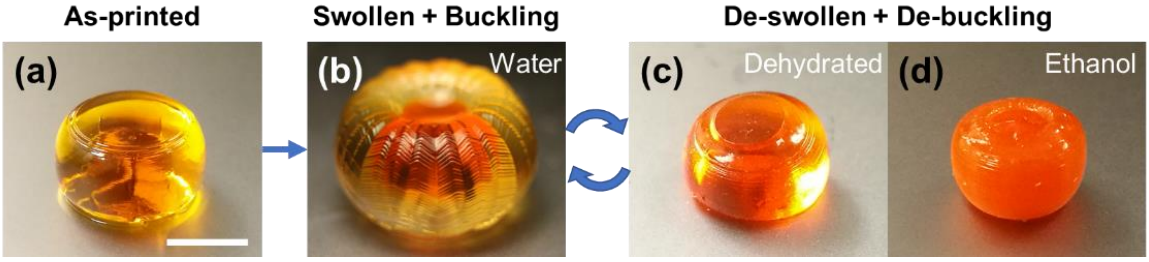

Figure S7. Different states of the printed 4s-10s pumpkin models: (a) as-printed state; (b) swollen and buckling state after immersion in water (c) shrunk state after dehydration in air; (d) shrunk state in ethanol. The scale bar is 5 mm.

References

(1) Hong, W.; Zhao, X.; Zhou, J.; Suo, Z. A theory of coupled diffusion and large deformation in polymeric gels. *Journal of the Mechanics and Physics of Solids* **2008,** *56* (5), 1779-1793, DOI: 10.1016/j.jmps.2007.11.010.

(2) Wang, X.; Zhai, Z.; Chen, Y.; Jiang, H. A facile, robust and versatile finite element implementation to study the time-dependent behaviors of responsive gels. *Extreme Mechanics Letters* **2018,** *22*, 89-97, DOI: 10.1016/j.eml.2018.05.007.

(3) Duan, Z., Jiaping Zhang, Yonghao An, and Hanqing Jiang. Simulation of the transient behavior of gels based on an analogy between diffusion and heat transfer. *Journal of Applied Mechanics* **2013,** *80* (4), 041017, DOI: 10.1115/1.4007789].

(4) Dervaux, J.; Couder, Y.; Guedeau-Boudeville, M. A.; Ben Amar, M. Shape transition in artificial tumors: from smooth buckles to singular creases. *Phys Rev Lett* **2011,** *107* (1), 018103, DOI: 10.1103/PhysRevLett.107.018103.

(5) Edward K. Rodriguez, A. H., Andrew D. McCulloch,. Stress-dependent finite growth in soft elastic tissues. *Journal of Biomechanics* **1994,** *27* (4), 455-467, DOI: 10.1016/0021-9290(94)90021-3.

(6) Jin, L.; Cai, S.; Suo, Z. Creases in soft tissues generated by growth. *EPL (Europhysics Letters)* **2011,** *95* (6), 64002, DOI: 10.1209/0295-5075/95/64002.